

RSC Advances



This is an *Accepted Manuscript*, which has been through the Royal Society of Chemistry peer review process and has been accepted for publication.

Accepted Manuscripts are published online shortly after acceptance, before technical editing, formatting and proof reading. Using this free service, authors can make their results available to the community, in citable form, before we publish the edited article. This *Accepted Manuscript* will be replaced by the edited, formatted and paginated article as soon as this is available.

You can find more information about *Accepted Manuscripts* in the [Information for Authors](#).

Please note that technical editing may introduce minor changes to the text and/or graphics, which may alter content. The journal's standard [Terms & Conditions](#) and the [Ethical guidelines](#) still apply. In no event shall the Royal Society of Chemistry be held responsible for any errors or omissions in this *Accepted Manuscript* or any consequences arising from the use of any information it contains.

Dissociation of oxygen on pristine and nitrogen-doped carbon nanotubes: a spin-polarized density functional study

Divya Srivastava^a, Toma Susi^{b,†}, Maryam Borghei^b and Laasonen Kari^{a*}

Although nitrogen-doped nanocarbon systems have recently received intense attention, the mechanism for the observed highly efficient oxygen reduction is still under debate. To address this issue, we investigated the adsorption and dissociation of an oxygen molecule on three pristine or nitrogen-doped nanocarbon systems: graphene, single-walled and double-walled carbon nanotubes using density functional theory calculations. The adsorption and dissociation energies were determined for both pristine and N-doped single-walled carbon nanotubes of different diameters with graphitic-like N substitutions in order to see the effect of diameter on oxygen dissociation. It was found that the energy barrier for oxygen dissociation, chemisorption energy and reaction energy are a function of carbon nanotube diameter, but independent of the number of walls. We also investigated the energy barrier of oxygen dissociation on single-walled carbon nanotubes with different types of nitrogen doping (i.e. pyridinic and graphitic). It was observed that higher nitrogen concentrations greatly reduce the energy barrier for graphitic nitrogen. Our results contribute towards a better understanding of the reaction mechanism for nitrogen-doped carbon nanomaterials involving oxygen molecule dissociation in the first step.

Introduction

Fuel cells are highly efficient and sustainable devices that generate electricity through an electrochemical reaction. In a fuel cell, oxygen reduction is one of the most important electrochemical reactions at the cathode. One of the serious problems in large scale commercialization of fuel cells is the high-cost, limited supply and poor durability of noble metal electrocatalysts (e.g. Pt, Pt-based alloys, Au and Ru) that are needed to accelerate the otherwise slow oxygen reduction reaction (ORR). Inexpensive electrocatalysts of high performance are therefore highly desired to help fuel cells reach their potential for power-related applications.

In recent years, a lot of research has been devoted to finding an efficient platinum-free catalyst. Recently, it was observed that metal-free nitrogen-doped carbon nanomaterials (N-CNM) such as carbon nanotubes (CNT) and graphene possess excellent catalytic activity for ORR¹⁻⁶. Moreover, these nanomaterials are inexpensive, catalytically long-lasting and have better tolerance toward CO poisoning compared to platinum catalysts. Although undoped carbon nanomaterials are excellent Pt-catalyst supports⁷, they are generally inert for ORR.

Doping carbon nanomaterials with nitrogen induces significant changes in their chemical and electronic properties that help enhance their ORR activity. But the chemical states and the role of nitrogen concentration in N-doped carbon nanomaterials are still under debate. XPS analysis has revealed that N-CNMs contain different nitrogen functionalities: nitrogen can be present in pyridinic, pyrrolic, pyridine-N-oxide or in graphitic forms^{2,8-11}. Although very recently the first atomically resolved measurements have started to shed light on local atomic configuration of nitrogen dopants in graphene¹²⁻¹⁵ and tentatively even in carbon nanotubes¹⁶, it is still not clear which configuration is responsible for the excellent electrocatalytic activity in these systems.

In many studies it has been reported that N-CNM with a higher concentration of pyridinic-type nitrogen or pyrrole/pyridine-type nitrogen exhibit a higher activity for ORR^{1-2,10-11}. However, Niwa et al. found that N-CNM containing more graphitic nitrogen compared to pyridinic nitrogen show higher ORR activity¹⁷. A theoretical study by Ni et al. has also supported these results¹⁸. However, other theoretical studies have suggested that the energy barrier of oxygen molecule (O₂) dissociation is smallest on nitrogen-doped Stone-Wales (SW) defects^{18,19}. Chao et al. suggested that pyridinic-like structures in highly curved graphitic layers become favorable as the concentration of nitrogen increases, while graphitic-like structures are dominant in less curved layers⁹. It is also reported that heat treatment transforms a particular type of nitrogen into other types which are more catalytically active for ORR⁸. Sharifi et al, showed that heat treatment of nitrogen-doped carbon nanotubes from 500 to 1000C leads to the transformation of pyrrolic functionalities into pyridinic-like functionalities followed by a transition into graphitic and proposed “quaternary-valley” nitrogen functionalities. They found the “quaternary-valley” nitrogen sites to be the most ORR active sites⁸. However, it should be noted that a higher proportion of graphitic sites implies a higher crystallinity of the nanotube structure (as would also be expected from heat treatments), which likely affects electron conduction and thus might affect the measured ORR activity.

Most theoretical calculations up to date have been done on single-walled nanotubes of very narrow diameters (less than 1 nm). This is not very realistic since most ORR studies have used multiwalled carbon nanotubes, having diameters in the range of 1 to 100 nm and several microns in length^{4,7,8,11}. In the present study, we have for the first time theoretically investigated the effect of tube diameter and the number of walls on the catalytic properties of nitrogen-doped carbon nanotubes. To study the effect of diameter, we considered single-walled nanotubes (SWNTs) with chiralities (8,0), (10,0), (16,0), (10,10) and (20,0), both pristine and doped with graphitic-like nitrogen (N-SWNTs). To further study the effect of wall number, we studied double-walled carbon nanotubes (10,0)@(20,0). Finally, we studied the effects of nitrogen concentration by including several N substitutions in the unit cell, and the effect of local bonding by including pyridinic-like nitrogen in the calculations.

Methods

Spin-polarized density functional theory (DFT) using a hybrid Gaussian and plane waves basis approach has been employed for the calculations, as implemented in the CP2K/QUICKSTEP²⁰ code. Spin-polarized DFT calculation is used to model the triplet state of O₂ and unpaired electrons.

In this method, a Gaussian-type basis is used to describe wave functions, while an auxiliary plane wave basis is used to describe the density. The Perdew, Burke and Ernzerhof (PBE)²¹ exchange-correlation functional within the generalized gradient approximation and norm-conserving Goedecker–Teter–Hutter (GTH)²² pseudopotentials were adopted. A plane wave cutoff of 500 Ry was used in the plane wave

expansion of the electron density. BFGS method has been used for the geometry optimization. Studied systems were relaxed until forces were less than $0.023\text{eV}\text{\AA}^{-1}$. The SWNTs used in this calculations are (n,0) zigzag SWNTs of 12.78 Å and (n,n) armchair SWNTs of length 12.298 Å along the tube axis direction. The climbing image nudged elastic band (CI-NEB) method²³ has been used to compute the minimum energy path and the activation barrier for oxygen dissociation. Eight to ten images have been interpolated between the initial and final states.

To evaluate the reliability of our CP2K/QUICKSTEP calculations, a comparative calculation was done with some of the N-SWNTs using GPAW code^{24,25} and a graphene sheet with CP2K and the Quantum Espresso (QE) software²⁶, which uses DFT based on plane waves and pseudo-potentials. The GPAW code uses grid as basis set and the PAW pseudo-potentials. The PBE exchange-correlation functional was used in all calculations. For QE calculations Vanderbilt ultrasoft pseudo-potentials were adopted. The energy cutoff of 450 Ry was taken to describe the plane wave basis. Geometry optimizations were performed with a $7\times 7\times 1$ Monkhorst–Pack k-point grid. Oxygen adsorption energies on the graphene sheet and a N-doped graphene sheet calculated from QE, CP2K and the GPAW results are given in Table 2. It can be seen that all the methods give very similar oxygen adsorption energies.

Results and discussions

In the following, we discuss the adsorption of an oxygen molecule on pristine and nitrogen-doped (one or more nitrogen) SWNTs and graphene. Oxygen adsorption on carbon nanomaterials has been characterized by three distinct states: a physisorbed state, a chemisorbed state and a dissociated state. In the physisorbed state, the carbon nanotube has a weak van der Waals interaction with the oxygen molecule. In this state O_2 remains in its triplet state, so there is no charge transfer between a O_2 and the carbon nanotube. In the chemisorbed state, the oxygen molecule forms a chemical bond with atoms of the carbon nanotube and loses its magnetic moment. Finally, in dissociative adsorption, the O-O bond of the oxygen molecule breaks and it dissociates into atomic oxygen. It is important to note that in nitrogen-doped SWNTs, O_2 adsorption takes place on a C-C site where one or two of the C atoms are adjacent to the nitrogen dopant. O_2 adsorption on C-N bridge site is not energetically favorable.

Graphitic nitrogen sites in single-walled carbon nanotubes

There are two sites for an oxygen molecule to adsorb on SWNT, the axial C-C site and the circumferential C-C site. Shan et al. have observed low activation barrier for O_2 dissociation on (10,0) zigzag SWNTs at axial C-C site¹⁹. For the armchair (10,10) SWNT, we calculate adsorption energies for both axial and circumferential C-C sites. The calculated chemisorption energies are 1.70 eV and 1.93 eV, respectively, and the reaction energies are 1.46 eV and 1.66 eV, respectively. Therefore, we only consider the axial C-C site for O_2 adsorption.

For O_2 adsorption on pristine SWNTs and N-SWNTs, first, we put an oxygen molecule on top of the axial C-C bond at a distance of 3.0 Å and performed geometry optimization, Fig. 1(a) and (b). In pristine SWNTs, the equilibrium distance of O_2 from the SWNT is in the range of 3.3 Å to 3.5 Å and the optimized O-O bond length ($d_{\text{O-O}}$) is 1.23 Å, Table 1. Our calculated $d_{\text{O-O}}$ with the PBE functional is consistent with a reported O-O equilibrium distance 1.23 Å also calculated with PBE²⁷. However, in case of N-SWNTs, the equilibrium distance of O_2 from N-SWNTs varies from 3.28 Å to 3.58 Å and $d_{\text{O-O}}$ is 1.24 Å or 1.25 Å which is slightly larger than that of pristine SWNT. Both C-O bond lengths ($d_{1\text{C-O}}$ and $d_{2\text{C-O}}$) are not of equal length. A C atom with N as a nearest neighbor has a shorter C-O bond length ($d_{2\text{C-O}}$) than other the carbon atom's bond length ($d_{1\text{C-O}}$). This holds for physisorbed, chemisorbed and dissociated states.

In order to investigate the chemisorption of O_2 on pristine and N-doped SWNTs, we decreased the distance between O_2 and the nanotubes. We put an oxygen molecule near the tube surface at a distance of around 1.5 Å. The optimized structural parameters are summarized in Table 1. As can be seen from Table 1, the length of the C-C bond on which O_2 is adsorbed is 1.53-1.59 Å, which indicates that it is a single bond rather than double bond. The bond length of O-O ($d_{\text{O-O}}$) is 1.50-1.52 Å. The O-O bond length is increased in the chemisorbed state from its value in the physisorbed state (1.23 Å), and is comparable to O-O single bond length (1.48 Å). The bond lengths of C-O (1.48-1.50 Å) are slightly longer than that of a C-O single bond (1.43 Å). Nevertheless, the C-O bond length is much shorter than the value of 3.32-3.58 Å found in the physisorbed state. These results clearly indicate that the O_2 molecule is chemisorbed on pristine and N-doped SWNTs and that its electronic ground state changes from a triplet state to a singlet state. The distance between O and C with a N neighbor is shorter than the C-O distance in pristine SWNTs, and is always shorter than other C-O bonds in N-SWNTs. This clearly indicates that there exists a strong interaction between O and C adjacent to the N atom that facilitates O_2 dissociation.

The chemisorbed oxygen molecule is adsorbed onto a tube surface into a preliminary state. O_2 then dissociates into atomic oxygens on opposite C-C sites of the tube axis, as shown in Figs. 1 (e) and (f). Dissociation of an oxygen molecule on different sides of the tube axis has been considered. Shan et al. found the lowest activation barrier for this type of dissociation in (10,0) SWNT and N-SWNT¹⁹. The detailed structural informations of all the studied SWNTs and N-SWNTs are listed in Table 1. To see the role of tube curvature on O_2 dissociation, we have calculated the chemisorption and reaction energies on SWNTs and N-SWNTs (see Table 2). We have taken the physisorbed energy as reference energy for the chemisorption and reaction energies, since in physisorption the electronic structure of the adsorbent and adsorbate is hardly perturbed. We have also calculated the activation barrier for O_2 dissociation on some of the studied pristine and N-doped SWNTs and also on graphene (see Table 2). One can observe from the data reported in Table 2 that the energy barrier for O_2 dissociation on pristine carbon nanomaterials is very high, making them chemically inert for O_2 dissociation.

By doping SWNTs and graphene with nitrogen in the graphitic configuration, we observe a decrease in their chemisorption energies, reaction energies (except for the (8,0) SWNT) and activation barriers. The effect of nitrogen doping on chemisorption energies is larger for narrow tubes (diameter less than or equal to 1 nm). For (8,0) and (10,0) SWNTs, the reductions in chemisorption energies are observed to be around 80% and 70%, respectively. For the larger diameter SWNTs (diameter greater than 1 nm) and graphene, reductions in chemisorption energies are observed in the range of 42% to 32%.

In Fig. 2(a), the chemisorption energies of O₂ on pristine and N-SWNTs are plotted against the tube curvature (inverse of radius). The reaction energy of larger diameter N-SWNTs is higher than narrow diameter N-SWNTs. For our studied larger diameter N-SWNTs, reaction energy is rather independent of tube curvature. However, it increases again to 1.11 eV for N-doped graphene. The reaction energies of O₂ on pristine and N-SWNTs as a function of the tube curvature are shown in Fig. 2 (b). Activation barriers for chemisorption of O₂ were calculated: 2.26 eV for (20,0) SWNT, 2.83 eV for graphene, 1.35 eV for (10,10) N-SWNT, and 1.33 eV for (20,0) N-SWNT. In all these cases it is observed that the activation barrier for chemisorption of O₂ is similar or lower than those of the activation barrier for oxygen dissociation. The lowest activation barrier of 0.88 eV for O₂ dissociation was observed for the (10,0) N-SWNT. Our results for the pristine and nitrogen-doped (10,0) SWNT are comparable with reported theoretical observations¹⁹. Ni et al. has reported that the activation barrier on a (8,0) N-SWNT is 0.86 eV¹⁸. The calculated activation barriers for O₂ dissociation are higher for larger diameter N-SWNTs and N-doped graphene than for narrow N-SWNTs, and are in the range of 1.37 eV to 1.81 eV. These observations suggest that the adsorption energy, the reaction energy and the activation barrier do depend on the nanotube curvature. We wanted to make sure that we had taken large enough unit cells in the direction of the tube axis to have a converged value for the total energy of the system. To this end, we made calculations for the (10,10) SWNT with a 1x1x10 unit cells (containing 400 carbon atoms). Comparing chemisorption and reaction energies with (10,10) SWNT containing 200 carbon atoms (see Table. 1). We obtained the same activation barrier of 1.37 eV for both N-doped (10,10) SWNTs (see Table 2).

The diameter, length and number of walls of a carbon nanotube depend on its growth process and treatment. To see the effect of number of walls on O₂ dissociation, we calculated the chemisorption and reaction energies for a double-walled carbon nanotube (10,0)@(20,0) (i.e. a (10,0) SWNT concentric inside a (20,0) SWNT), and compared that to the empty (20,0) case. It can be seen from the data summarized in Table 2, that there is not much of an effect of the second wall on O₂ dissociation.

The electronic properties of SWNTs are mostly depends on two parameters: (1) diameter of the nanotube, and (2) whether the nanotube is metallic or semiconducting. White et al. have shown²⁸ that all semiconducting SWNTs (achiral zigzag (n,0) and chiral (n₁,n₂)) with similar diameters will have similar density of states (DOS) in the vicinity of the Fermi energy (E_F). They also gave an analogous correspondence for metallic nanotubes²⁸. In other words, it is independent of the chiral angle. The chiral and achiral carbon nanotubes with n₁-n₂≠3q, q is an integer, will have band-gaps inversely proportional to the diameter of the nanotube. Therefore, when the semiconducting carbon nanotube diameter increases the band gap shrinks and the tube become metallic²⁹. In the case of nitrogen-doped SWNTs, nitrogen atom has one more valance electron than carbon atom. The substitution of N into SWNTs would induce donor level near the bottom of the conduction band. Therefore, semiconducting N-SWNT becomes either metallic or narrow-gap semiconductor. The main effect of the nitrogen doping in DOS of carbon nanotube is raising the states close-above the E_F. In order to correlate it with the activation barrier of O₂ dissociation, electron rich nitrogen atom increase the charge transfer capability of the adjacent carbon atom, which enhances the dissociation of O₂ on carbon nanotube and reduces the activation barrier^{19,30}.

In order to study the effect of metallicity of zigzag tube on oxygen dissociation, we calculate O₂ adsorption energies for (9,0) and (18,0) N-SWNTs with diameter 7.046Å and 14.09Å, respectively. On the basis of diameter, we can put the (9,0) in between of (8,0) and (10,0) tubes and (18,0) in between the (10,10) and the (20,0) tubes. The chemisorption energy and reaction energy of (9,0) N-SWNT are -0.223 eV and -0.267 eV, respectively. It can be seen from Table. 2 that (9,0) N-SWNT has lower chemisorption and reaction energy than (8,0) N-SWNT. The calculated chemisorption and reaction energy of (18,0) N-SWNT are 0.84 eV and 0.134 eV. It has lower chemisorption and reaction energies than N-SWNTs (16,0) and (10,10) (see Table.2). However, narrow semiconducting zigzag tube (diameter < 1 nm) has lower chemisorption energy than larger diameter metallic tube (see Fig 2(a)). The larger diameter metallic (18,0) and narrow semiconducting (8,0) and (10,0) N-SWNTs have almost same reaction energy for O₂ dissociation (see Fig 2(b)). Higher O₂ adsorption energies for metallic (10,10) N-SWNT than the metallic zigzag (18,0) N-SWNT, is related to their different geometry. Metallic property of tube helps in O₂ dissociation, even though tube diameter is key parameter for O₂ dissociation.

It is interesting to note that we observe a new local minimum (Fig. 3(c)) in the minimum energy pathways (MEP) between an initial (chemisorbed, Fig 3(a)) and a final (dissociated, Fig 3(b)) state. This minimum is observed in (10,0), (10,10), and (20,0) N-SWNTs and in N-doped graphene. These minimum have lower energy than those of the final local minimum. The reaction energies increase with increase in radius of N-SWNTs, given in Table 2 inside braces. For graphene, both minima have approximately the same reaction energy. In the final state (Fig 3(b)) of these systems, the C atom next to the N dopant involved in O₂ dissociation has a C-N bond length 1.46-1.47 Å (see Table 1). This clearly indicates that there exists a single bond between them. In the minimum (Fig. 3(c)), the distance between the C taking part in O₂ adsorption and the adjacent N atom are 2.53, 1.65, 2.07, and 1.56 Å for (10,0), (10,10), (20,0) N-SWNTs and N-doped graphene, respectively. The C-N bond lengths are larger than the C-N distance in a single bond (1.465 Å). Thus, in effect, the O₂ dissociation breaks the C-N bond and dynamically converts N from graphitic into the pyridinic configuration. Considering this minimum as a final configuration and the chemisorption state as initial configuration, we have calculated the MEP. The activation barriers for two different final states: graphitic N (E^{G-like}), Fig 3(b) and pyridinic N (E^{P-like}), Fig 3(c), are almost same (see Table 2).

In order to try to find an even lower activation barrier for O₂ dissociation, we selected the (10,10) SWNT of diameter 1.356 nm for a further study. A number of theoretical and experimental works have revealed that nitrogen concentration in nitrogen-doped carbon nanomaterials plays an important role for catalytic activity^{9, 10, 18}. We therefore considered five different isomers of a (10,10) SWNT with two graphitic nitrogen dopants (N₂-SWNT), as shown in Fig. 4. In the isomers, C atoms are substituted by N atoms so that the nitrogen atoms are third-nearest neighbors (3-N₂-SWNT_1 and 3-N₂-SWNT_2), second-nearest neighbors (2-N₂-SWNT) and first-nearest neighbors (1-N₂-SWNT_1, 1-N₂-SWNT_2). The optimized configurations of physisorbed, chemisorbed and dissociated states of O₂ on I-N₂-SWNT (I=1,2,3) tubes are displayed in Fig. 4 and the corresponding chemisorption energy and reaction energy are listed in Table 3. It is found that O₂ can enter into a stable chemisorption state on N-SWNTs when two nitrogen atoms are not directly bonded, while O₂ adsorption on N₂-SWNTs with two nitrogen atoms adjacent to one another (1-N₂-SWNT_1 and 1-N₂-SWNT_2) are energetically less favorable. For 3-N₂-SWNT_2 isomers, two different dissociation path have been studied, see Fig.4 (ii) (c) and Fig 4(ii) (c'), and their reaction energies given in Table 3. Lower reaction energy is observed for a dissociation path in which O atoms dissociate on C-C bridge sites next to N atoms (Fig.4

(ii) (c)). In the optimized structures of isomers 1-N2-SWNT_1 (Fig.4 (iv)) and 1-N2-SWNT_2 (Fig.4 (v)), the distances between nitrogen atoms are 1.47 Å and 1.49 Å, respectively. This clearly indicates that there exists a single bond between two nitrogen atoms for both the isomers. We did not observe N-N bond breaking during the structure optimization of isomer 1-N2-SWNT_1, and therefore no aromatic $(4n+2)$ π system formation, as has been observed for this isomer of a (5,5) SWNT³¹. Our finding suggests that their conjecture may be valid only for narrow armchair nanotubes. In the case of N2-SWNT tubes, the most stable chemisorbed and dissociated states are observed for the 2-N2-SWNT isomer. This type of a double substitution in which two N atoms are next-nearest neighbors was recently observed in N-doped graphene¹³.

We will discuss the 2-N2-SWNT isomer in more detail. The distance between an oxygen in O₂ and the C atom adjacent to two N atoms (or another C atom) are 2.96 (3.26), 1.45 (2.54) and 1.23 (1.45) Å in physisorbed, chemisorbed and dissociated states, respectively, see Fig. 4(iii). The chemical interaction stretches the O-O bond length from 1.25 Å to 1.38 Å which is shorter than the O-O single bond length (1.48 Å). In the dissociated state, one O atom adsorbed on the top site of a C atom (adjacent to the two N atoms) and the other O atom is adsorbed along the C-C bridge site. In its optimized dissociated state, we note that the N atoms attain bond lengths of 1.64 and 1.68 Å with the C atom adjacent to two N atoms, slightly larger than the length of a typical C-N single bond (1.465 Å). The C-N bond lengths of both the N atoms with other carbon atoms are 1.36-1.38 and 1.37-1.39 Å. Therefore, O₂ dissociation on a 2-N2-SWNT transforms graphitic nitrogen atoms into pyridinic ones. The length of the C-C bond on which O₂ is adsorbed is 1.51 Å.

The activation barrier for oxygen dissociation is around 0.183 eV, substantially lower than the 1.37 eV barrier on the (10,10) N-SWNT. It is important to note that in this case, we did not get any activation barrier for chemisorption of O₂. It can be seen from the data in Table 2 and Table 3 that chemisorption energies and O₂ reaction energies are lower in the N2-isomer of the (10,10) SWNT. Therefore, a higher nitrogen concentration can significantly reduce the chemisorption energy and reaction energy, which helps in lowering the activation barrier.

Pyridinic-like nitrogen doping in (10,10) single-walled carbon nanotube

For pyridinic-like N-doping in the (10,10) SWNT, two different kind of local structures are considered. The first structure contains a vacancy surrounded by three nitrogen atoms (N3V-SWNT). In the other structure, divacancies is surrounded by four nitrogen atoms (N4V2-SWNT). First, we discuss the adsorption and dissociation of O₂ on the N3V-SWNT tube. For O₂ adsorption, we consider three possible adsorption sites: O₂ molecule sitting above the (i) C2-C3 site (N3V-SWNT_1), (ii) C5-C6 site (N3V-SWNT_2) and, (iii) C1-C2 site (N3V-SWNT_3), see Fig. 5.

For the N3V-SWNT_1 tube, two different O₂ dissociation paths are considered. In one case the O₂ molecule dissociates along the C2-C1 and C3-C4 bridge sites (symmetric), while in the other case, O₂ dissociation takes place on the C2-C1 and C3-C5 bridge sites (asymmetric). The lowest reaction energy (0.513 eV) is observed for the symmetric dissociation path. In N3V-SWNT_2, the O₂ molecule dissociates along the C5-C3 carbon bond and on top of the C6 atom. In N3V-SWNT_3, O₂ dissociates along the C2-C3 bond and on the C1 atom. The calculated chemisorption energies and O₂ reaction energies in N3V-SWNTs are high and listed in Table 4. Among all the possible configurations, the lowest chemisorption energy (1.14 eV) and reaction energy (0.513 eV) are observed for the N3V-SWNT_1 configuration, similar to the graphitic-like nitrogen-doped (10,10) SWNT (Table 2).

Next, we examined O₂ adsorption and dissociation on the N4V2-SWNT tube. We put the O₂ molecule above the C-C bond site neighboring the N dopants. The optimized configurations of O₂ adsorption and dissociation are displayed in Fig. 6 and the chemisorption energy and reaction energy are listed in Table 4. In the optimized structures, the C-O bond lengths are 3.45, 3.54 and 1.39, 1.39 Å for the physisorbed state and the chemisorbed state, respectively. The O-O bond length is elongated from 1.23 to 1.50 Å. In the chemisorbed state, it is found that the C-C bond on which the O₂ molecule is adsorbed is broken. This chemisorbed state is stable with chemisorption energy of -0.22 eV. Finally, for oxygen dissociation, we considered two different configurations: in the first configuration, oxygen dissociation occurs on C-C sites adjacent to a N dopant, see Fig. 6(c), and in the other, one oxygen atom is adsorbed on a C-C bridge site neighboring the N dopant and the other on the C-C bridge site two sites away from the N dopant, see Fig. 6(c'). It is interesting to note that the lengths of the C-C bond on which oxygen (O) is adsorbed are 2.14 Å and 2.10-2.12 Å for both dissociation configurations, Figs. 6(c) and 6(c'), respectively. This indicates that there is no chemical bond between the two C atoms on which O is adsorbed. The dissociation configuration shown in Fig. 6(c) has a lower reaction energy (0.278 eV) than the configuration shown in Fig. 6(c') (0.524 eV). The oxygen dissociation barrier for the configuration corresponds to lower reaction energy is 0.602 eV which is slightly lower than the observed barrier for N-SWNT. However, a high activation barrier of around 2.3 eV for chemisorption of O₂ was found in this configuration. Such a high barrier is likely due to the breaking of the C-C bond (2.72 Å) on which the O₂ molecule is chemisorbed and the formation of the resulting sixteen atoms ring (including the four N atoms), instead of the tetra-atomic ring (C-O-O-C) observed in all other studied chemisorbed states. Therefore, the overall energy barrier of N4V2-SWNT is higher than the N-SWNT. Thus, N-SWNTs with vacancies (single and divacancies) and pyridinic-like nitrogen atoms have higher activation barriers than graphitic-like nitrogen-doped SWNT. Nevertheless, their barriers are still lower than in pristine SWNTs.

Bader charge analysis

In order to understand the reduced energy barrier on nitrogen-doped SWNTs, a charge analysis was performed using Bader analysis³²⁻³⁴, based on the electronic charge density. Table 5 reports atomic charge values of C atoms adjacent to N atoms and the N atoms for N-SWNT, N2-SWNTs and N4V2-SWNT. We see that on nitrogen doping of SWNTs, the 2p electrons of C atoms are transferred to adjacent N atoms, which creates a net positive charge on the C atoms. The positively charged C atoms strongly interact with O atoms, favoring O₂ dissociation. The positive charge densities on C atoms bonded to the N dopant in axial and circumferential directions are asymmetric (see Table 5). Doping of N into the SWNT modifies the tube structure by a rearrangement of the nearest neighbor carbon atoms. This give rise to different C-N bond-lengths in the direction perpendicular to tube axis and the direction making an angle with the tube axis, and may result in different charges on the carbon atoms.

The finding that the lowest activation barrier was found for 2-N2-SWNT than for any of the other studied N-doped SWNTs with same or different concentrations or types of nitrogen can be understood by the charge analysis. In the 2-N2-SWNT, one of the two carbon

atoms on which the O₂ molecule is adsorbed has two N atoms as nearest neighbors. This makes this C atom (C11, see Table 5) much more positively charged than other C atoms having one or zero adjacent N atoms (see Table 5). This results in a low activation barrier.

On the basis of the charge analysis we can also understand the formation of the sixteen-atom ring in O₂ chemisorption on the N4V2-SWNT tube. In this case, N atoms are in pyridinic configurations; i.e., N atoms are bonded with two C atoms. A C atom adjacent to a nitrogen atom in a pyridinic configuration is more positively charged than a C atom adjacent to a N atom in a graphitic configuration (see Table 5). When the O₂ molecule is adsorbed on the C11-C21 bond, these carbon atoms form strong bond with the O atoms with bond lengths of 1.39 Å (smaller than the C-O bond length in N-SWNTs and N2-SWNTs). Therefore the C11-C21 bond breaks and a sixteen-atoms ring forms.

Conclusions

In summary, the adsorption of an oxygen molecule on pristine and N-doped carbon nanomaterials has been investigated using density functional theory calculations. It was observed that pristine carbon nanomaterials are inert towards O₂ dissociation. By nitrogen doping, the electrochemical activities of these materials towards the oxygen reduction reaction ORR could be enhanced. Our theoretical investigations suggest that nanotube curvature has strong affect to the oxygen dissociation activation energy barrier. Narrow (< 1 nm) N-SWNTs exhibit much lower activation barriers for O₂ dissociation compared to the larger diameter N-SWNTs and N-doped graphene. The curvature has strong influence to the O₂ adsorption but also the orientation of the SWNT will have effect to the O₂ adsorption. The metallic zigzag N-SWNT with almost same diameter has lower adsorption energy than that of the semiconducting zigzag N-SWNT.

We also found that O₂ dissociation on SWNTs and graphene with a single substitutional nitrogen atom can lead to the transformation of graphitic nitrogen configurations into pyridinic ones. Such transformations are also observed when two N atoms are substituted into the SWNT. SWNTs with graphitic-like nitrogen have a lower overall energy barrier for O₂ adsorption than those with a higher concentration of pyridinic-like nitrogen. However, when a SWNT has two graphitic-like nitrogen atoms, the energy barrier can be as low as 0.18eV, much lower than the lowest barrier of 1.37 eV we found for a N-SWNT with a single graphitic-like nitrogen. On the basis of these results we conclude that the energy barrier of O₂ adsorption on nitrogen-doped carbon nanomaterials decreases with increasing concentration of graphitic-like nitrogen atoms. Thus our investigation helps in understanding the specific role of carbon nanotube curvature, nitrogen concentration and types of nitrogen doping in ORR activity.

Acknowledgements

This work was supported by Academy of Finland Centre of Excellence function by COMP. We would like to thank Dr. Tanja Kallio for useful discussions of the N-CNT usage in fuel cells. Divya Srivastava thanks CSC-IT Center for Science, for providing high-performance computing facilities.

Table 1 Optimized d_{O-O} , d_{1C-O} , d_{2C-O} and d_{C-N} bond lengths, as shown in Fig 1, of studied pristine and N-doped SWNTs and graphene sheet.

Systems SWNT(n,m)	Physisorbed state		Chemisorbed state		Dissociate state		
	Pristine	N-doped	Pristine	N-doped	Pristine	N-doped	
(8,0)	Diameter =6.26Å						
	d_{O-O} (Å)	1.23	1.24	1.50	1.51	2.92	2.84
	d_{1C-O} (Å)	3.32	3.42	1.48	1.50	1.45	1.44
	d_{2C-O} (Å)	3.32	3.18	1.48	1.45	1.45	1.43
	d_{C-C} (Å)	1.42	1.40	1.53	1.53	1.48	1.49
	d_{C-N} (Å)	-	1.43	-	1.50	-	1.47
(10,0)	Diameter=7.830Å						
	d_{O-O} (Å)	1.23	1.24	1.51	1.50	2.89	2.82
	d_{1C-O} (Å)	3.39	3.58	1.48	1.50	1.45	1.45
	d_{2C-O} (Å)	3.39	3.55	1.48	1.46	1.45	1.42
	d_{C-C} (Å)	1.43	1.41	1.53	1.53	1.48	1.49
	d_{C-N} (Å)	-	1.42	-	1.49	-	1.47
(16,0)	Diameter=12.529Å						
	d_{O-O} (Å)	1.23	1.25	1.52	1.50	2.85	2.73
	d_{1C-O} (Å)	3.49	3.20	1.50	1.53	1.45	1.42
	d_{2C-O} (Å)	3.49	3.07	1.50	1.48	1.47	1.35
	d_{C-C} (Å)	1.43	1.42	1.54	1.54	1.49	1.53
	d_{C-N} (Å)	-	1.41	-	1.48	-	1.56
(10,10)	Diameter=13.563Å						
	d_{O-O} (Å)	1.23	1.25	1.51	1.50	3.06	3.02
	d_{1C-O} (Å)	3.39	3.30	1.48	1.53	1.46	1.46
	d_{2C-O} (Å)	3.36	3.06	1.49	1.47	1.46	1.42
	d_{C-C} (Å)	1.42	1.41	1.59	1.57	1.51	1.46
	d_{C-N} (Å)	-	1.41	-	1.46	-	1.46
(20,0)	Diameter=15.661Å						
	d_{O-O} (Å)	1.23	1.24	1.50	1.50	2.83	2.79
	d_{1C-O} (Å)	3.39	3.28	1.50	1.53	1.46	1.46
	d_{2C-O} (Å)	3.36	3.29	1.50	1.47	1.45	1.42
	d_{C-C} (Å)	1.42	1.42	1.53	1.53	1.49	1.49
	d_{C-N} (Å)	-	1.41	-	1.48	-	1.47
Graphene	Diameter=Infinity						
	d_{O-O} (Å)	1.24	1.25	1.51	1.50	2.84	2.80
	d_{1C-O} (Å)	3.68	3.54	1.50	1.54	1.46	1.46
	d_{2C-O} (Å)	3.68	3.27	1.50	1.48	1.46	1.42
	d_{C-C} (Å)	1.42	1.42	1.53	1.54	1.48	1.49
	d_{C-N} (Å)	-	1.41	-	1.47	-	1.46

Table 2 Calculated chemisorption energies, reaction energies and O₂ dissociation activation barriers on pristine and one N atom substituted SWNTs and graphene. Physisorption energy was used as the reference energy. See Fig. 1.

SWNTs	Chemisorption Energy (eV)	Reaction energy (eV)	Activation Barrier (eV)	
			E ^{G-like}	E ^{P-like}
(8,0)	0.65	0.07	-	-
(10,0)	1.51	0.31	2.01 [1.97] ^a	-
(16,0)	1.99	0.98	-	-
(10,10) with 200 atoms	1.70	1.46	-	-
(10,10) with 400 atoms	1.90	1.38	-	-
(20,0)	1.68	1.00	2.43	-
DWNT (10,0@20,0)	1.70	1.04	-	-
Graphene	2.257 (2.33 _{QE}) ^{**}	1.88(2.0 _{QE}) ^{**}	(3.31 _{QE}) [*] [2.71] ^b	-
				-
N-SWNTs				
(8,0)	0.12	0.15	-	-
(9,0)	-0.223	-0.267	-	-
(10,0)	0.46 (0.38 _{GP}) ^{**}	0.09 {-1.06} [*] (-0.06 _{GP}) ^{**}	0.88 [0.68] ^a	0.98
(16,0)	1.23	0.68	-	-
(10,10) with 200 atoms	1.01 (0.77 _{GP}) ^{**}	0.68 (0.25 _{GP}) ^{**}	1.372	-
(10,10) with 400 atoms	1.09	0.54 {-0.46} [*]	1.37	1.373
(18,0)	0.84	0.134	-	-
(20,0)	1.01	0.68{-0.28} [*]	1.46	1.369
N-DWNT (10,0@20,0)	1.02	0.675	-	-
N-graphene	1.52 (1.54 _{QE}) ^{**}	1.11 (1.19 _{QE}) ^{**} ({1.17} [*] _{QE}) ^{**}	(1.81 _{QE}) ^{**} [1.87] ^b	(1.857 _{QE}) ^{**}

† Data enclosed in square brackets are taken from references: ^aRef. 18 and ^bRef. 19.

*Data in braces are calculated reaction energies for pyridinic configurations. **Data in parentheses are calculated by using Quantum Espresso (QE) or GPAW (GP) package.

^{G-like} Graphitic configuration. ^{P-like} pyridinic configuration.

Table 3 Calculated chemisorption energies, reaction energies and O₂ dissociation activation barriers on two N atom substituted (10,10) SWNT (N2-SWNT). Physisorption energy was used as the reference energy. See Fig. 3.

Isomers	Chemisorption (eV)	Reaction Energy (eV)	Activation Barrier (eV)
3-N2-SWNT_1	-0.1167	-0.512	
3-N2-SWNT_2	-0.064	0.2244 ^a 0.3567 ^b	
2-N2-SWNT	-0.158	-1.559	0.183
1-N2-SWNT_1	0.404	-0.9156	
1-N2-SWNT_2	0.440	-0.4686	

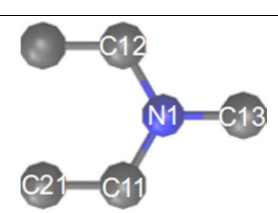
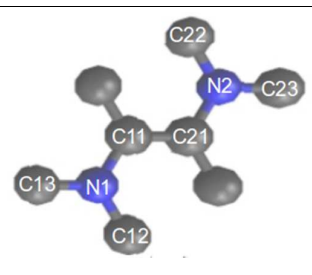
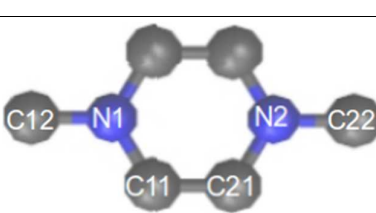
† ^aReaction energy of 3-N2-SWNT_2, shown in Fig.3 (ii)(c) and ^breaction energy of 3-N2-SWNT_2 shown in Fig.3 (ii)(c').

Table 4 Calculated chemisorption energies, reaction energies and O₂ dissociation activation barriers on (10,10) SWNT with pyridinic-like N atoms. Physisorption energy was used the reference energy. N3V-SWNT: three pyridinic N atoms with single vacancy (see Fig. 4). N4V2-SWNT: four pyridinic N atoms with di-vacancy (see Fig. 5).

System/Configurations	Chemisorption (eV)	Reaction Energy (eV)	Activation Barrier (eV)
N3V-SWNT_1	1.1445	0.512 ^a , 0.873 ^b	-
N3V-SWNT_2	1.835	1.399	-
N3V-SWNT_3	1.754	1.0297	-
N4V2-SWNT	-0.215	0.2785 ^c , 0.524 ^d	0.602 (2.3)*

† The two values in the third column correspond to reaction energies for two different dissociation paths. ^aO₂ molecule dissociates along C2-C1 and C3-C4 bridge sites, Fig. 4 and ^bO₂ dissociation takes place on C2-C1 and C3-C5 bridge sites, Fig.3. ^cDissociated state shown in Fig. 5(c) and ^d dissociated state shown in Fig. 5(c'). *The value in parentheses is the energy barrier for chemisorption.

Table 5 Atomic charges of C and N atoms (in units of electron charge) in pristine and nitrogen-doped (10,10) SWNTs.

System (10,10)	Atoms	Atomic Charges	Net Charge	Sites of atoms in SWNT
SWNT	C	4	0	
N-SWNT	N1 C11 C12 C13 C21	7.19 3.11 3.11 3.67 3.997	-2.19 +0.89 +0.89 +0.33 +0.003	
3-N2-SWNT_1	N1 N2 C11 C21 C12 C13 C22 C23	7.67 7.59 3.00 3.28 3.15 3.23 3.16 3.21	-2.67 -2.59 +1.0 +0.72 +0.85 +0.77 +0.84 +0.79	
3-N2-SWNT_2	N1 N2 C11 C21 C12 C22	7.15 7.60 3.07 3.27 3.61 3.06	-2.15 -2.60 +0.93 +0.73 +0.39 +0.94	

2-N2-SWNT	N1	7.64	-2.64	
	N2	7.49	-2.49	
	C11	1.796	+2.20	
	C21	3.95	+0.05	
	C12	3.41	+0.59	
	C13	3.23	+0.59	
	C22	3.41	+0.59	
	C23	3.21	+0.79	
N4V2-SWNT	N1	7.85	-2.85	
	N2	7.82	-2.82	
	N3	7.75	-2.75	
	N4	7.74	-2.74	
	C11	2.62	+1.38	
	C12	2.63	+1.37	
	C21	2.43	+1.57	
	C22	2.61	+1.39	
	C31	2.57	+1.43	
	C32	2.61	+1.39	
	C41	2.75	+1.25	
	C42	2.60	+1.40	

† O₂ molecule adsorbed at C11-C21 site.

Notes and references

^aDepartment of Chemistry, Aalto University, P.O. Box 16100, 00076 Aalto, Finland

^bDepartment of Applied Physics, Aalto University, P.O. Box 15100, 00076 Aalto, Finland

[†]Present address: University of Vienna, Faculty of Physics, Strudlhofgasse 4, A-1090 Vienna, Austria

*Corresponding Author: kari.laasonen@aalto.fi

1. L. T. Qu, Y. Liu, J. B. Baek and L. M. Dai, *ACS Nano*, 2010, **4**, 1321-1326.
2. K. Gong, F. Du, Z. Xia, M. Durstock and L. Dai, *Science*, 2009, **323**, 760–764.
3. L. Zhang and Z. Xia, *J. Phys. Chem. C*, 2011, **115**, 11170-11176.
4. H. Li, H. Liu, Z. Jong, W. Qu, D. Geng, X. Sun and H. Wang, *Int. J. Hydrogen Energy*, 2011, **36**, 2258–2265.
5. G. B. Sumpster, et al. *ACS Nano*, 2007, **1**, 369-375.
6. Maryam Borghei, et al., Highly active Nitrogen-containing few-walled carbon nanotubes with very low nitrogen content for oxygen reduction reaction. *Submitted*.
7. C. Wnag, M. Waje, M. J. Tang, C. R. Haddon and Y. Yan, *Nano Letters*, 2004, **4**, 345-348.
8. T. Sharifi, G Hu, X. Jia and T. Wågberg, *ACS Nano*, 2012, **6**, 8904–8912.
9. J. Y. Chao et al., *J. Phys. Chem. C*, 2011, **115**, 3737-3744.
10. V. C. Rao, R. C. Cabrera and Y. Ishikawa, *J. Phys. Chem. Lett.*, 2010, **J**, 2622-2627.
11. S. Kundu, T. C. Nagaiah, W. Xia, Y. Wang, S. V. Dommele, J. H. Bitter, M. Santa, G. Grundmeier, M. Bron, W. Schuhmann et al., *J. Phys. Chem. C*, 2009, **113**, 14302–14310.
12. Liuyan Zhao, Rui He, Kwang Taeg Rim, Theanne Schiros, Keun Soo Kim, Hui Zhou, Christopher Gutiérrez, S. P. Chockalingam, Carlos J. Arguello, Lucia Pálková, Dennis Nordlund, Mark S. Hybertsen, David R. Reichman, Tony F. Heinz, Philip Kim, Aron Pinczuk, George W. Flynn, Abhay N. Pasupathy, *Science*, 2011, **333**, 999–1003.
13. Ruitao Lv, Qing Li, Andrés R. Botello-Méndez, Takuya Hayashi, Bei Wang, Ayse Berkdemir, Qingzhen Hao, Ana Laura Elías, Rodolfo Cruz-Silva, Humberto R. Gutiérrez, Yoong Ahm Kim, Hiroyuki Muramatsu, Jun Zhu, Morinobu Endo, Humberto Terrones, Jean-Christophe Charlier, Minghu Pan, and Mauricio Terrones, *Sci. Rep.* 2012, **2**, 586.
14. Rebecca J. Nicholls, Adrian T. Murdock, Joshua Tsang, Jude Britton, Timothy J. Pencycook, Antal Koós, Peter D. Nellist, Nicole Grobert, and Jonathan R. Yates, *ACS Nano*, 2013, **7**, 7145-7150.
15. U. Bangert, William Pierce, D. M. Kepaptsoglou, Quentin M. Ramasse, R. Zan, M. H. Gass, J. A. Van den Berg, C. B. Boothroyd, J. Amani, and H. Hofsäss, *Nano Lett.*, 2013, **13(10)**, 4902-4907.
16. Y. Tison, H. Lin, J. Lagoute et al., *ACS Nano*, 2013, **7**, 7219-7226.
17. H. Niwa, K. Horiba, Y. Harada, M. Oshima, T. Ikeda, K. Terakura, J. Ozaki and S. Miyata, *J. Power Sources*, 2009, **187**, 93–97.
18. S. Ni, Z. Li and J. Yang, *Nanoscale*, 2012, **4**, 1184.
19. B. Shan and K. Chao, *Chem. Phys. Lett.* 2010, **492**, 131-13.
20. J. VandeVondele, M. Krack, F. Mohamed, M. Parrinello, T. Chassaing, J. Hutter, *Comput. Phys. Commun.* 2005, **167**, 103.
21. J. P. Perdew, K. Burke and M. Ernzerhof, *Phys. Rev. Lett.* 1996, **77**, 3865-3868.
22. S. Goedecker, M. Teter and J. Hutter, *Phys. Rev. B*, 1996, **54**, 1703.
23. G. Henkelman, B. P. Uberuaga, H. Jonsson, *J. Chem. Phys.*, 2000, **113** (22), 9901-9904.
24. J. J. Mortensen, L. B. Hansen, and K. W. Jacobsen, *Physical Review B*, 2005, **71**, 035109
25. J. Enkovaara, et al., *J. Phys.: Condens. Matter*, 2010, **22**, 253202
26. P. Giannozzi et al, *J. Phys.: Condens. Matter*, 2009, **21** 395502.
27. P. Giannozzi, R. Car and G. Scoles, *J. Chem. Phys.*, 2003, **118**, 1003-1006.
28. C. T. White and J. W. Mintmire, *Nature (London)*, 1998, **394**, 29.
29. C. T. White, D. H. Robertson, and J. W. Mintmire, *Phys. Rev. B*, 1993, **47**, 5485-5488
30. Jae-Yel Yi and J. Bernholc, *Phys. Rev. B*, 1993, **47**, 1708-1711.
31. S. H. Kang and S. Jeong, *Phys. Rev. B*, 2004, **70**, 233411.
32. G. Henkelman, A. Arnaldsson, H. Jónsson, *Comput. Mater. Sci.*, 2006, **36**, 254-360.
33. E. Sanville, S. D. Kenny, R. Smith and G. Henkelman, *J. Comp. Chem.* 2007, **28**, 899-908.
34. W. Tang, E. Sanville and G. Henkelman, *J. Phys.: Condens. Matter* 2009, **21**, 08420.

Figure captions:

Fig. 1 Oxygen adsorption on pristine SWNT and SWNT with a graphitic-like nitrogen dopant (N-SWNT). O₂ physisorption on (a) SWNT and (b) N-SWNT, O₂ chemisorption on (c) SWNT and (d) N-SWNT, and dissociated oxygen (e) SWNT and (f) N-SWNT.

Fig. 2 Oxygen adsorption energies are plotted against the tube curvature, (a) chemisorption energy, (b) reaction energy. **The metallic zigzag N-SWNTs have lower chemisorption energy and reaction energy than those semiconducting N-SWNTs with similar diameter.** The black and blue solid circles represent pristine and N-doped carbon nanomaterials (SWNTs and graphene), respectively. The dashed lines are guides to the eye.

Fig. 3 Structures of the (a) initial and (b) final local minima for the minimum energy pathway (MEP) calculations. (c) Structure of the observed new local minima in the MEP.

Fig. 4 Optimized configurations of O₂ (a) Physisorbed configuration, (b) Chemisorbed configuration, (c) Dissociated oxygen, (c') O₂ dissociated on C atoms two bonds apart from N atom, on isomers of doubly N substituted (10,10) SWNT: (i) 3-N2-SWNT_1, (ii) 3-N2-SWNT_2, (iii) 2-N2-SWNT, (iv) 1-N2-SWNT_1, and (v) 1-N2-SWNT_2. The carbon, nitrogen and oxygen atoms are represented by gray, blue and red color spheres, respectively.

Fig. 5 Structure of pyridinic-like doping of nitrogen atoms on the (10,10) SWNT with three nitrogen atoms surrounding a vacancy (N3V-SWNT). C1, C2, C3, C4, C5, and C6 are the adsorption sites for O₂.

Fig. 6 Optimized configurations of O₂ adsorption and dissociation on the N4V2-SWNT tube: (a) Physisorbed state, (b) Chemisorbed state, (c) and (c') Two different dissociated states. The carbon, nitrogen and oxygen atoms are illustrated using gray, blue and red color spheres, respectively.

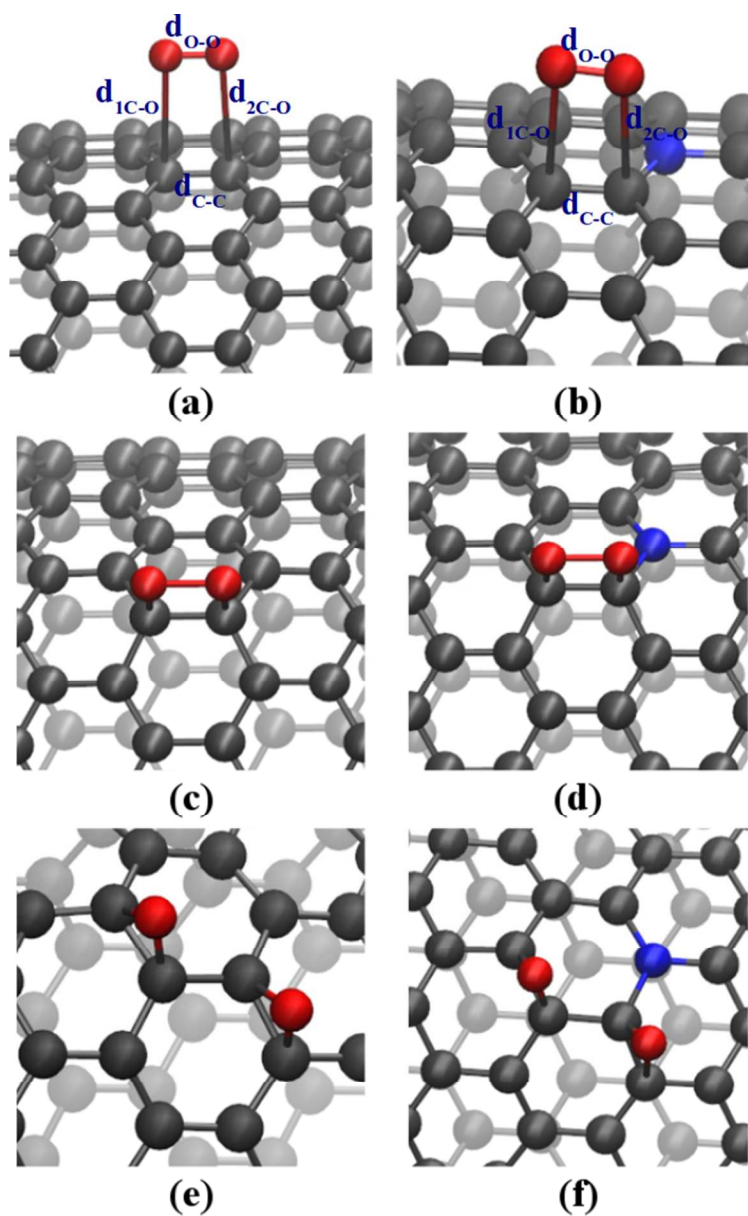


Fig. 1 Oxygen adsorption on pristine SWNT and SWNT with a graphitic-like nitrogen dopant (N-SWNT). O₂ physisorption on (a) SWNT and (b) N-SWNT, O₂ chemisorption on (c) SWNT and (d) N-SWNT, and dissociated oxygen (e) SWNT and (f) N-SWNT.

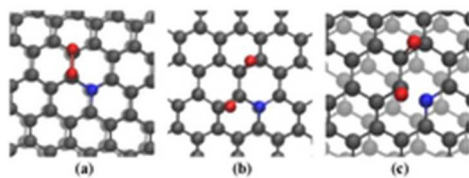


Fig. 3 Structures of the (a) initial and (b) final local minima for the minimum energy pathway (MEP) calculations. (c) Structure of the observed new local minima in the MEP.
19x7mm (300 x 300 DPI)

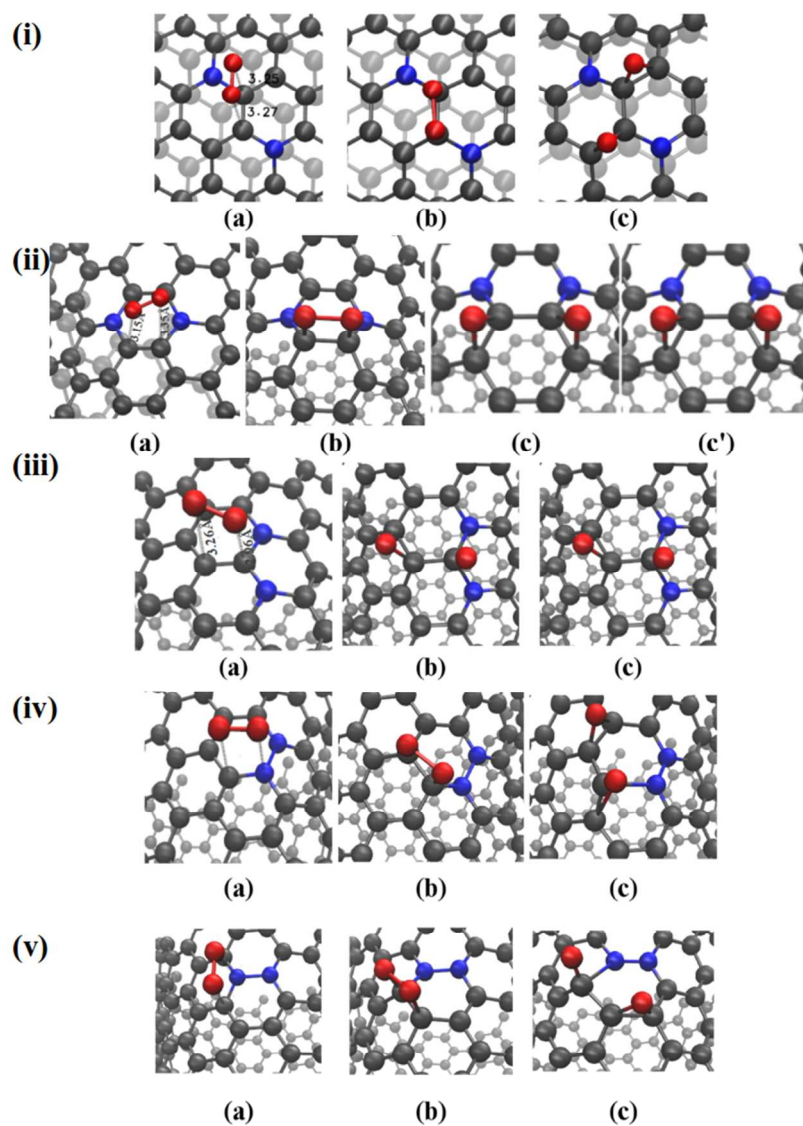


Fig. 4 Optimized configurations of O₂ (a) Physisorbed configuration, (b) Chemisorbed configuration, (c) Dissociated oxygen, (c') O₂ dissociated on C atoms two bonds apart from N atom, on isomers of doubly N substituted (10,10) SWNT: (i) 3-N₂-SWNT_1, (ii) 3-N₂-SWNT_2, (iii) 2-N₂-SWNT, (iv) 1-N₂-SWNT_1, and (v) 1-N₂-SWNT_2. The carbon, nitrogen and oxygen atoms are represented by gray, blue and red color spheres, respectively.

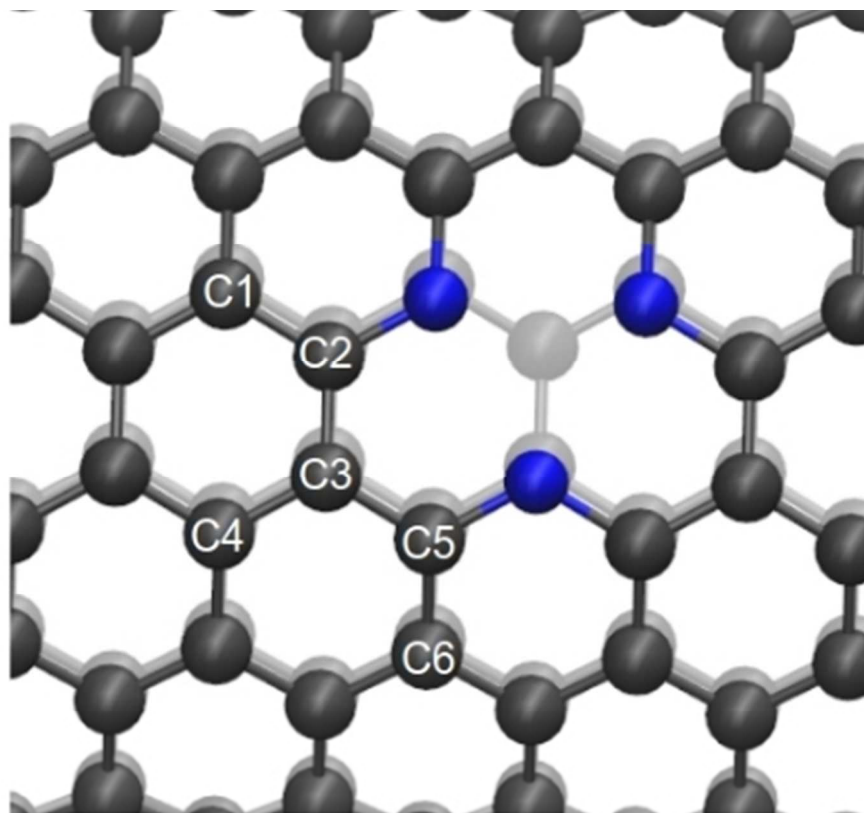


Fig. 5 Structure of pyridinic-like doping of nitrogen atoms on the (10,10) SWNT with three nitrogen atoms surrounding a vacancy (N3V-SWNT). C1, C2, C3, C4, C5, and C6 are the adsorption sites for O₂.
155x143mm (72 x 72 DPI)

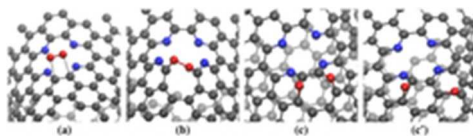
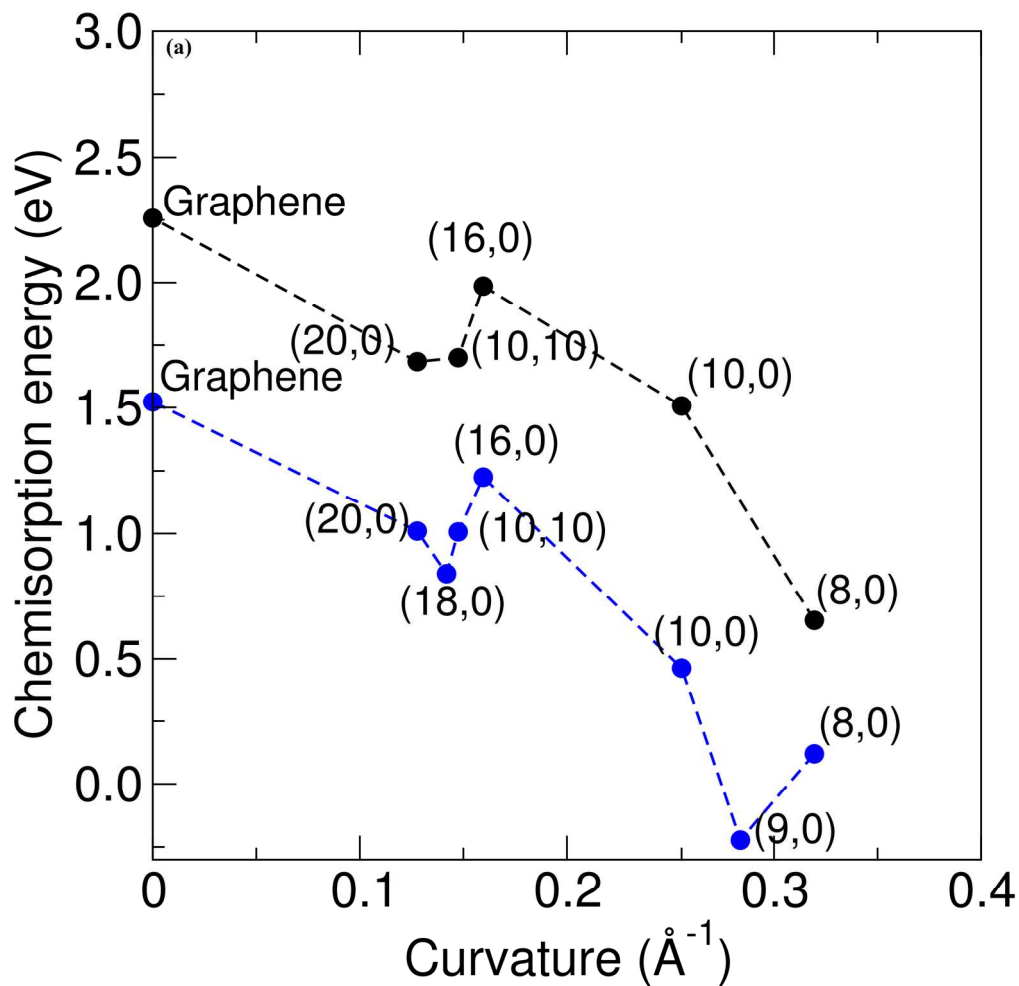
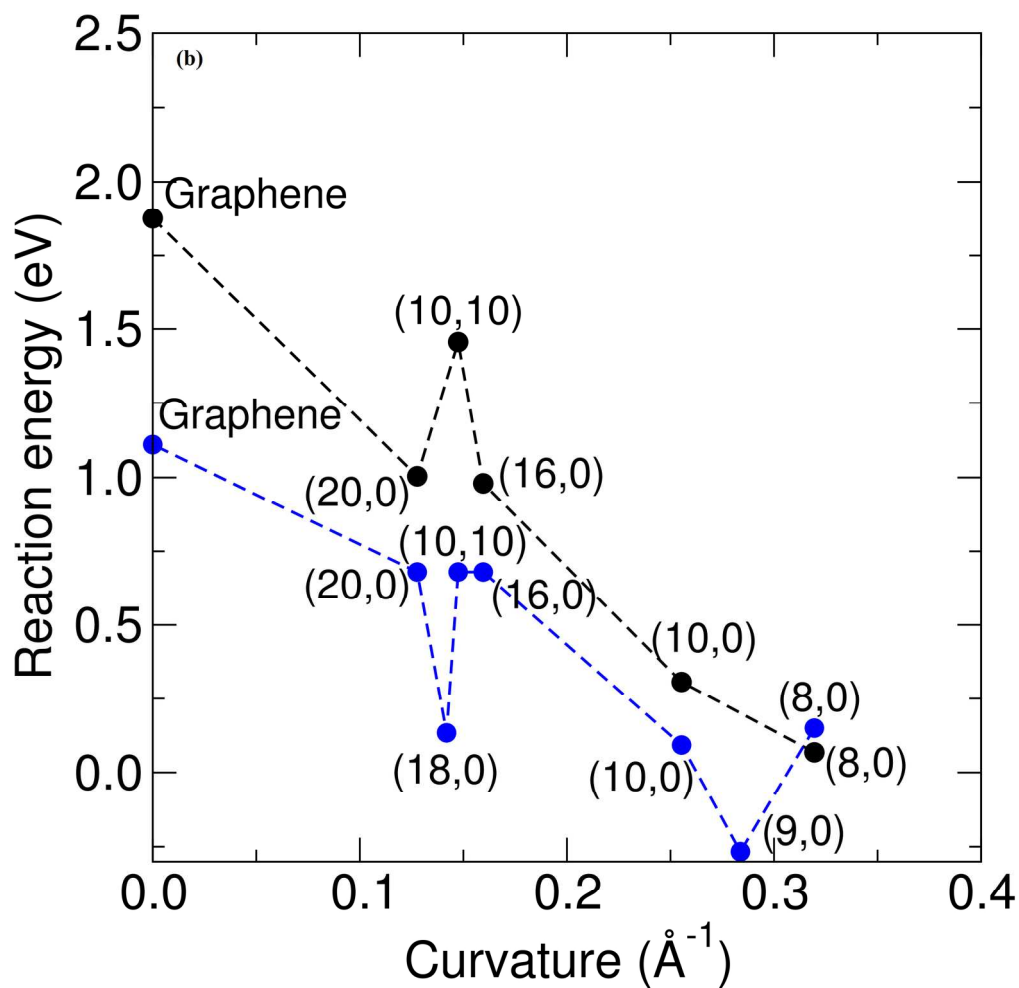


Fig. 6 Optimized configurations of O₂ adsorption and dissociation on the N₄V₂-SWNT tube: (a) Physisorbed state, (b) Chemisorbed state, (c) and (d) Two different dissociated states. The carbon, nitrogen and oxygen atoms are illustrated using gray, blue and red color spheres, respectively.
19x5mm (300 x 300 DPI)



Oxygen adsorption energies are plotted against the tube curvature, (a) chemisorption energy, (b) reaction energy. The metallic zigzag N-SWNTs have lower chemisorption energy and reaction energy than those semiconducting N-SWNTs with similar diameter. The black and blue solid circles represent pristine and N-doped carbon nanomaterials (SWNTs and graphene), respectively. The dashed lines are guides to the eye.
177x172mm (300 x 300 DPI)



Oxygen adsorption energies are plotted against the tube curvature, (a) chemisorption energy, (b) reaction energy. The metallic zigzag N-SWNTs have lower chemisorption energy and reaction energy than those semiconducting N-SWNTs with similar diameter. The black and blue solid circles represent pristine and N-doped carbon nanomaterials (SWNTs and graphene), respectively. The dashed lines are guides to the eye.

177x172mm (300 x 300 DPI)